# Time-dependent System Reliability Analysis with Second Order

## **Reliability Method**

### Hao Wu

Graduate Research Assistant

School of Mechanical Engineering

Purdue University

West Lafayette, IN, 47907, United States

E-mail: wu1508@purdue.edu

### Xiaoping Du

Professor

Department of Mechanical and Energy Engineering

Indiana University - Purdue University Indianapolis,

723 W. Michigan Street

Indianapolis, IN, 46202, United States

E-mail: duxi@iu.edu

### Zhangli Hu

**Graduate Research Assistant** 

Department of Mechanical and Aerospace Engineering

Missouri University of Science and Technology

Rolla, MO, United States

E-mail: zh3zd@mst.edu

#### **ABSTRACT**

System reliability is quantified by the probability that a system performs its intended function in a period of time without failures. System reliability can be predicted if all the limit-state functions of the components of the system are available, and such a prediction is usually time consuming. This work develops a time-dependent system reliability method that is extended from the component time-dependent reliability method using the envelope method and second order reliability method. The proposed method is efficient and is intended for series systems with limit-state functions whose input variables include random variables and time. The component reliability is estimated by the second order component reliability method with an improve envelope approach, which produces a component reliability index. The covariance between component responses are estimated with the first order approximations, which are available from the second order approximations of the component reliability analysis. Then the joint distribution of all the component responses is approximated by a multivariate normal distribution with its mean vector being component reliability indexes and covariance being those between component responses. The proposed method is demonstrated and evaluated by three examples.

#### 1. INTRODUCTION

System reliability is measured by the probability that the system performs its intended function in routine circumstances during a specified period of time [1]. It is necessary to predict system reliability accurately and efficiently in the early design stage since it can be used to estimate the lifecycle cost, determine maintenance policies, and optimize the system performance [2-4]. A mechanical system consists of multiple components, and each component may also have multiple failure modes. In this work, we consider a failure mode as a component. If the limit-state function of a failure mode is invariant over time, its reliability and probability of failure are constant. However, the limit-state function may vary over time in many engineering problems, such as function generator mechanisms [5] and bridges under stochastic loading [6]. Then a time-dependent reliability method is required.

Suppose the limit-state function of the *i*-th failure mode is given by

$$Y_i = g_i(\mathbf{X}, t) \tag{1}$$

where  $Y_i$  is a component response, which is a function of time t;  $\mathbf{X} = (X_1, ..., X_n)^T$  is the vector of independent input random variables. Then the time-dependent component reliability on a time interval  $[t_0, t_s]$  is defined by

$$R(t_0, t_s) = \Pr(g(\mathbf{X}, t) \ge 0, \forall t \in [t_0, t_s])$$
(2)

and the corresponding probability of failure is defined by

$$p_f(t_0, t_s) = \Pr(g(\mathbf{X}, t) < 0, \exists t \in [t_0, t_s])$$
(3)

Eq. (3) indicates that if  $g(\cdot) < 0$  at any instant of time on  $[t_0, t_s]$ , the component fails.

In this study, we focus on series system. For a series system, the entire series system fails if one failure mode occurs. For a time-dependent series system, the system fails if any failure mode occurs at any instant of time. The system reliability  $R_s(t_0, t_s)$  and probability of system failure  $p_{fs}(t_0, t_s)$  are given by

$$R_s(t_0, t_s) = \Pr\left(\bigcap_{i=1}^m g_i(\mathbf{X}, t_i) \ge 0, \forall t_i \in [t_0, t_s]\right)$$

$$\tag{4}$$

and

$$P_{fs}(t_0, t_s) = \Pr\left(\bigcup_{i=1}^{m} g_i(\mathbf{X}, t_i) < 0, \exists t_i \in [t_0, t_s]\right)$$
 (5)

where  $\cup$  and  $\cap$  stand for union and intersection, respectively.

Component reliability analysis is required for system reliability analysis. Methods of time-dependent component reliability analysis include three groups: Rice's formula based methods [7-10], meta-model based methods [11-14], and methods which convert time-dependent into time-independent reliability. Rice's formula based methods are most commonly used [15]. For example, the PHI2 method [8] allows for time-variant reliability problems to be solved using classical time-invariant reliability method, the first order reliability method (FORM). Hu and Du then proposed the joint up-crossing rate method in estimating the time-dependent reliability [9]. Rice's formula-based methods are in general more efficient than others but may lead to large errors if up-crossings are strongly dependent.

Higher accuracy can be achieved by metamodeling methods. Hu and Du introduced a mixed efficient global optimization method employing the adaptive Kriging-Monte Carlo simulation (MCS) so that this high accuracy is achieved [13]. Wang and Wang developed a nested extreme response surface method by employing Kriging for reliability analysis with time-variant performance characteristics [14]. This group of methods may result in a high computational cost if the dimension of the problem is high.

Converting a time-dependent problem into a time-independent counterpart is possible by using the extreme value of the limit-state function. The methods include the envelope function method [16], extreme value response method [17], and the composite limit-state function method [18]. Still, obtaining accurate distribution of the extreme value in an efficient way is complicated. Hu and Du recently employed sequential efficient global optimization (EGO) to transform the time-dependent reliability problem into a time-independent problem with a second order method. The Hessian matrix is approximated by a quasi-Newton approach. It uses the gradients of the limit-state function at the points before the MPP search converges to the MPP. The method is efficient, but it may not accurately approximate the Hessian matrix since the points may not be on the surface of the envelope function [19].

Many studies have been conducted on time-dependent system reliability as well. For instance, Song and Der Kiureghian developed a joint first-passage probability method based on the conditional distribution analysis in estimating the reliability of systems subjected to stochastic excitation [20]. Radhika et al. investigated nonlinear vibrating systems under stochastic excitations by implementing the asymptotic extreme value theory and Monte Carlo simulation (MCS) [21]. Yu et al. employed the combination of the extreme value moment and improved maximum entropy method to access the time-variant system reliability with temporal parameters [22]. Gong and Frangopol proposed a new efficient method for time-dependent reliability which is formulated as a large-scale series system consisting of time-independent response functions [23]. Hu and Mahadevan proposed a novel and efficient methodology for time-dependent system reliability by considering the system as an equivalent Gaussian random field [24]. Jiang and Wei introduced an improved time-variant reliability analysis method based on stochastic process discretization,

which transformed the time-variant reliability problem into time-invariant series system problem [25].

Time-independent system reliability can be approximated by the multidimensional integration of the joint probability density function (PDF) of random variables once the marginal distributions and correlation coefficients of component states are obtained by the second and first order approximations [26]. Wu and Du proposed a method of predicting the time-independent system reliability by approximating the marginal distributions with the second order saddlepoint method (SOSPA) [27].

It is desirable to take advantages of methods for both time-dependent component reliability and time-independent system reliability. To this end, in this work we integrate the second order saddlepoint approximation [19] for both time-dependent component reliability and time-independent system reliability. The distinctive feature of our new method is the ture second order approximation to component envelope functions with its accurate Hessian matrix calculation. The second derivatives of the envelope functions with repsect to the input random variables are exactly evaluated from the second derivatives of the corresponding component limit-state functions with respect to the input random variables and time. The second feature is that the second order approaxiamtion is extended from component reliability analysis to system reliability analysis.

This paper is organized as follows: Section 2 reviews the first order reliability method for time dependent reliability analysis. Section 3 discusses the proposed method for time-dependent system reliability analysis. Section 4 presents three examples, and Section 5 provides conclusions and discusses possible future work.

#### 2. METHODOLOGY REVIEW

The second order time-dependent system reliability method is based on several existing methods, which are reviewed in this section.

### 2.1 Time-Dependent Component Reliability

The limit-state function of a component is given in Eq. (1), and its reliability is therefore a function of time (or timespan) as indicated in Eq. (2). The most commonly used reliability method is FORM, which is reviewed below.

#### 2.1.1 First Order Reliability Method

FORM is originally used for time-independent reliability analysis, and it can also be used for time-dependent reliability analysis. It converts a general non-Gaussian process response into an equivalent Gaussian process response.  $\mathbf{X}$  is at first transformed into standard normal variables  $\mathbf{U}$ . Then the most probable point (MPP)  $\mathbf{u}^*$  at t is identified by the following model:

$$\begin{cases}
\min \sqrt{\mathbf{U}^{\mathrm{T}}\mathbf{U}} \\
\text{s. t. } g(\mathbf{X}, t) = g(\mathbf{T}(\mathbf{U}), t) = 0
\end{cases}$$
(6)

where  $T(\cdot)$  is an operator of the transformation from **U** to **X**.

The limit-state function is linearized at  $\mathbf{u}^*(t)$  by

$$g(\mathbf{T}(\mathbf{U}),t) = g(\mathbf{u}^*,t) + \sum_{i=1}^{N} \frac{\partial g}{\partial U_i} \bigg|_{\mathbf{u}^*} (U_i - u_i^*)$$

$$= \nabla g(\mathbf{u}^*,t)(\mathbf{U} - \mathbf{u}^*)$$
(7)

where  $\nabla g(\mathbf{u}^*, t) = \left[\frac{\partial g}{\partial U_1}\Big|_{\mathbf{u}^*}, \dots, \frac{\partial g}{\partial U_N}\Big|_{\mathbf{u}^*}\right]$  is the gradient, and  $u_i^*$  is the *i*-th component of  $\mathbf{u}^*$ .

Then the probability of failure is computed by

$$p_f = \Pr(g(\mathbf{X}, t) < 0, \exists t \in [t_0, t_s]) \tag{8}$$

= 
$$Pr(\beta(t) + \alpha(t)\mathbf{U} < 0, \exists t \in [t_0, t_s])$$

where  $\beta(t)$  is the time-dependent reliability index, given by

$$\beta(t) = \|\mathbf{u}^*\| \tag{9}$$

and  $\alpha(t)$  is the time-dependent unit gradient vector given by

$$\alpha(t) = \frac{\nabla g(t)}{\|\nabla g(t)\|} = [\alpha_1(t), \alpha_2(t), \dots, \alpha_N(t)]$$
(10)

As Eq. (7) shows, the non-Gaussian process  $g(\mathbf{X}, t)$  has been transformed into an equivalent Gaussian process represented as a sum of standard normal random variables. After this, many methodologies are available for solving for the probability of failure, such as the upcrossing rate method [8, 9] and MCS [28].

### 2.1.2 Sequential optimization with EGO [19]

The time-dependent probability of failure can be evaluated by the extreme value of the limitstate function.

$$p_f(t_o, t_s) = \Pr(g(\mathbf{X}, t) < 0, \exists t \in [t_o, t_s])$$

$$= \Pr\left(\min_{t \in [t_o, t_s]} g(\mathbf{X}, t) < 0\right)$$
(11)

The extreme limit-state function is equivalent to the envelope function [16] or the composite limit-state function [18], and  $\min_{t \in [t_o, t_s]} g(\mathbf{X}, t)$  is obtained by

$$G(\mathbf{X}) = \min_{t \in [t_0, t_s]} g(\mathbf{X}, t) = g(\mathbf{X}, \tilde{t}(\mathbf{X}))$$
(12)

where  $G(\mathbf{X})$  is the global minimum value of  $g(\mathbf{X}, t)$  with respect to t.  $G(\mathbf{X})$  is time independent and only depends on  $\mathbf{X}$ .  $\tilde{t}$  is the time instant when the global minimal value of  $G(\mathbf{X})$  occurs.  $\tilde{t}$  is the function of  $\mathbf{X}$ .

$$\tilde{t} = \left\{ \tilde{t} \mid \min_{t \in [t_0, t_s]} g(\mathbf{X}, t) \right\}$$
(13)

The envelope function  $G(\mathbf{X})$  is a surface tangent to all the instantaneous limit-state functions at different time instants. If FORM is used for envelope function, its MPP is obtained by

$$\begin{cases} \min \sqrt{\mathbf{U}^{\mathrm{T}}}\mathbf{U} \\ \text{s. t.} \min_{t \in [t_{o}, t_{s}]} g(\mathbf{T}(\mathbf{U}), t) = 0 \end{cases}$$
 (14)

Eq. (14) is a double loop optimization problem. The inner loop is the global optimization with respect to time t while the outer loop is the MPP search with respect to  $\mathbf{U}$ . The double loop is decoupled into a sequential single-loop process.

The first cycle is FORM analysis, the MPP  $\mathbf{u}_{(1)}^*$  at the initial time  $t_0$  by

$$\begin{cases}
\min \sqrt{\mathbf{U}^{\mathrm{T}}\mathbf{U}} \\
\text{s. t. } g(\mathbf{T}(\mathbf{U}), t_{0}) = 0
\end{cases}$$
(15)

Then the time is updated by global optimization at  $\mathbf{u}_{(1)}^*$ , and the new time is denoted by  $\tilde{t}^{(1)}$ , which is given by

$$\tilde{t}^{(1)} = \operatorname*{argmin}_{t \in [t_o, t_s]} g\left( T(\mathbf{u}_{(1)}^*, t) \right)$$
(16)

In the next cycle, the new MPP  $\mathbf{u}_{(2)}^*$  is located at the time instant  $\tilde{t}^{(1)}$  using Eq. (16). And then the time is updated to  $\tilde{t}^{(2)}$  by performing global optimization at  $\mathbf{u}_{(2)}^*$ .

$$\tilde{t}^{(2)} = \underset{t \in t_0, t_s]}{\operatorname{argmin}} g\left(T(\mathbf{u}_{(2)}^*, t)\right)$$
(17)

The above process is repeated until convergence.

The Efficient Global Optimization (EGO) is employed to solve the time t [29]. EGO has been widely used in various areas because it can efficiently search for the global optimum [13, 30]. The task is to solve for the time so that  $g(t) = g(T(\mathbf{u}_{MPP}), t)$  is minimized. With a number of training points, the function is approximated by the following surrogate model:

$$\hat{y} = g(t) = g(T(\mathbf{u}_{MPP}), t) = F(t)^{\mathrm{T}} \gamma + Z(t)$$
(18)

where  $F(t)^{T}\gamma$  is a deterministic term, F(t) is a vector of regression functions,  $\gamma$  is a vector of regression coefficients, and Z(t) is a stationary Gaussian process with zero mean and a covariance given by

$$Cov(Z(t_1), Z(t_2)) = \sigma_Z^2 R(t_1, t_2)$$

$$\tag{19}$$

where  $\sigma_Z^2$  is process variance, and  $R(\cdot, \cdot)$  is the correlation function.

The output of the surrogate model is a Gaussian random variable following

$$\hat{y} = g(t) \sim N(\mu(t), \sigma^2(t))$$
(20)

where  $\mu(t)$  and  $\sigma(t)$  are the mean and standard deviation of  $\hat{y}$ , respectively.

After building the initial model, the expected improvement (EI) metric is used to identify the new training point with the highest probability to produce a better extreme value of the response.

The improvement is defined by

$$I = \max(y^* - y, 0) \tag{21}$$

where  $y^* = \min_{i=1,2,...,k} g(t_i)$  is the current minimum response.

EI is computed by

$$EI(t) = E[max(y^* - y, 0)]$$
(22)

$$= \left(y^* - \mu(t)\right) \Phi\left(\frac{y^* - \mu(t)}{\sigma(t)}\right) + \sigma(t) \phi\left(\frac{y^* - \mu(t)}{\sigma(t)}\right)$$

where  $\Phi(\cdot)$  and  $\phi(\cdot)$  are the cumulative distribution function (CDF) and PDF of a standard normal variable, respectively.

The new training point  $t_{new}$  is identified as the time that minimizes the expected improvement.

$$t_{new} = \underset{t}{\operatorname{argminEI}}(t) \tag{23}$$

The convergence criterion of EGO is set to  $\varepsilon_{EI} = |y^*| \times 2\%$ . By combining sequential strategy with EGO, the MPP  $\mathbf{u}^*$  of extreme limit-state function  $G(\mathbf{X})$  can be obtained efficiently by solving Eq. (14). The probability of failure with FORM is estimated by

$$p_f(t_o, t_s) = \Pr(g(\mathbf{X}, t) < 0, \exists t \in [t_o, t_s])$$

$$= \Pr(G(\mathbf{X}) < 0) = \Phi(-\beta)$$
(24)

where  $\beta = \| \mathbf{u}^* \|$  is the first order reliability index.

In general, the envelope function can be highly nonlinear and FORM may not be accurate enough. Thus, a second order method is preferred, and it uses the envelope theorem to obtain the second order information of the extreme limit-state function. Then SOSPA is used to estimate the probability of failure.

#### 3. PROPOSED METHOD

#### 3.1 Overview

The envelope function of a component (or limit-state function) is generally nonlinear as shown in Fig. 1. It is the reason we use a second order approximation for the envelope function. Specifically, we approximate the envelope function at its MPP with a quadratic function. As a result, we also need the gradient and the Hessian matrix of the envelope function at the MPP.

It is shown that the MPP of the envelope function is the worst-case MPP of the limit-state function on  $[t_0, t_s]$  [19]. In other words, the MPP is the closest point between the origin and all the instantaneous limit-state functions on  $[t_0, t_s]$ . This is illustrated in Fig. 1. The MPP of the envelope function can be efficiently found using the sequential single loop method [19]. This MPP is also the MPP of the worst-case limit-state function; as a result, the gradient of the envelope function is equal to the gradient of the worst-case limit-state function [19].

Place Fig. 1 here

Fig. 1 Relationship between the worst-case limit-state function and envelope function

The curvature of the envelope function, however, may not be the curvature of the worst-case limit-state function as shown in Fig. 1. This means that the Hessian matrix of the envelope function is in general not equal to that of the worst-case limit-state function. The Hessian matrix of the envelope function is approximated by the gradients of the instantaneous limit-state functions in [19], but the second derivative of the envelope function with respect to time is omitted. Hence the method in [19] may not always work. In this work, we derive analytical second derivatives of the envelope function with respect to both random input variables and time, and the Hessian matrix of the envelope function can then be obtained accurately.

The general procedure of finding the second order information of the envelope is summarized below. At first we employ the method in [19] to find the MPP of the envelope function using Eq. (14). Once we find the MPP, we know the gradient of the envelope function because it is equal to the gradient of the limit-state function at the MPP. Next we determine the Hessian matrix of the envelope function with Eq. (35). The Hessian matrix consists of second derivatives of the limit-state function with respect to random input variables  $\mathbf{X}$  and time t. The equations are derived in Sec. 3.2. When the MPP, gradient and Hessian matrix are available, we use the second order saddlepoint approximation to find the probability of component failure and then perform system reliability analysis. The method hereby is denoted by SOSPA.

### 3.2 Hessian matrix of the envelope function

After the MPP of the envelope function is found, a quadratic envelope function is formulated as[27]

$$G(\mathbf{U}) = \mathbf{a} + \mathbf{b}^{\mathrm{T}}\mathbf{U} + \mathbf{U}^{\mathrm{T}}\mathbf{C}\mathbf{U}$$
 (25)

where

$$\begin{cases} a = \frac{1}{2} (\mathbf{u}^*)^{\mathrm{T}} \mathbf{H} \mathbf{u}^* - \nabla G (\mathbf{u}^*)^{\mathrm{T}} \mathbf{u}^* \\ \mathbf{b} = \nabla G (\mathbf{u}^*) - \mathbf{H} \mathbf{u}^* \\ \mathbf{C} = \frac{1}{2} \mathbf{H} = \operatorname{diag}(\tilde{c}_1, \tilde{c}_2, \dots, \tilde{c}_N) \end{cases}$$
(26)

 $\nabla G(\mathbf{u}^*) = \left(\frac{\partial G}{\partial U_1}\Big|_{\mathbf{u}^*}, \dots, \frac{\partial G}{\partial U_n}\Big|_{\mathbf{u}^*}\right)^{\mathrm{T}}$  is the gradient of the envelope function. **H** is the Hessian

matrix, which is given by

$$\mathbf{H} = \begin{bmatrix} \frac{\partial^2 G}{\partial U_1^2} & \cdots & \frac{\partial^2 G}{\partial U_1 \partial U_n} \\ \vdots & \ddots & \vdots \\ \frac{\partial^2 G}{\partial U_n \partial U_1} & \cdots & \frac{\partial^2 G}{\partial U_n^2} \end{bmatrix}_{\mathbf{u}^*}$$
(27)

The envelope function  $G(\mathbf{X}) = 0$  at  $\mathbf{u}^*$  is given by

$$G(\mathbf{U}) = \min_{t \in [t_0, t_s]} g(\mathbf{U}, t) = g(\mathbf{U}, \tilde{t})|_{\mathbf{u}^*}$$
(28)

 $\tilde{t}$  is the worst-case time instant, and it is found by

$$\dot{g}(\mathbf{U},t) = 0 \tag{29}$$

where  $\dot{g}$  is the derivative of g with respect to t.

The first derivative of  $G(\mathbf{U})$  with respect to a random input variable at  $\mathbf{u}^*$  is

$$\frac{\partial G}{\partial U_i} = \frac{\partial g}{\partial U_i} + \frac{\partial g}{\partial \tilde{t}} \frac{\partial \tilde{t}}{\partial U_i} \tag{30}$$

As  $\dot{g}(\mathbf{U},t) = 0$ , Eq. (30) becomes

$$\frac{\partial G}{\partial U_i} = \frac{\partial g}{\partial U_i} \tag{31}$$

Eq. (31) indicates that the envelope function and the limit-state function have the same gradient at  $\mathbf{u}^*$ . Then, the second derivative of  $G(\mathbf{U})$  with respect random input random variables at  $\mathbf{u}^*$  is

$$\frac{\partial^2 G}{\partial U_i \partial U_j} = \frac{\partial}{\partial U_j} \left( \frac{\partial G}{\partial U_i} \right) = \frac{\partial}{\partial U_j} \left( \frac{\partial g}{\partial U_i} \right) 
= \frac{\partial^2 g}{\partial U_i \partial U_j} + \frac{\partial^2 g}{\partial U_i \partial t} \frac{\partial t}{\partial U_j} \tag{32}$$

We then take the derivative of Eq. (29) with respect to  $U_j$ , and it is given by

$$\frac{\partial \dot{g}}{\partial U_j} + \frac{\partial \dot{g}}{\partial t} \frac{\partial t}{\partial U_j} = 0 \tag{33}$$

$$\frac{\partial t}{\partial U_j} = -\frac{\partial \dot{g}}{\partial U_j} / \frac{\partial \dot{g}}{\partial t} \tag{34}$$

Plugging Eqs. (29) and (34) into Eq. (32) yields the Hessian matrix **H** at  $\mathbf{u}^*$  and  $\tilde{t}$ .

$$\frac{\partial^{2} G}{\partial U_{i} \partial U_{j}} \bigg|_{\mathbf{u}^{*}, \tilde{t}} = \frac{\partial^{2} g}{\partial U_{i} \partial U_{j}} \bigg|_{\mathbf{u}^{*}, \tilde{t}} - \frac{\partial^{2} g}{\partial U_{i} \partial t} \frac{\partial^{2} g}{\partial U_{j} \partial t} \bigg/ \frac{\partial^{2} g}{\partial t^{2}} \bigg|_{\mathbf{u}^{*}, \tilde{t}}$$
(35)

The finite difference method can be used to calculate the Hessian matrix of the envelope function.

Next, the second order saddlepoint approximation is employed to estimate the probability of failure. Saddlepoint approximation has several excellent features. It yields an accurate probability estimation, especially in the tail area of a distribution [31, 32].

The cumulant generating function (CGF) of  $G(\mathbf{U})$  is given by

$$K(s) = -\beta s + \frac{1}{2}s^2 - \frac{1}{2}\sum_{i=1}^{n-1}\log(1 - 2sk_i)$$
(36)

where  $k_i = \tilde{c}_i$ 

The derivatives of CGF are

$$K'(s) = -\beta + s + \sum_{i=1}^{n-1} \frac{k_i}{1 - 2sk_i}$$
(37)

$$K''(s) = 1 + \sum_{i=1}^{n-1} \frac{k_i^2}{(1 - 2sk_i)^2}$$
 (38)

The saddlepoint  $s_s$  is obtained by solving the following equation:

$$K'(t) = -\beta + s + \sum_{i=1}^{n-1} \frac{k_i}{1 - 2sk_i} = 0$$
 (39)

Then the probability of failure is evaluated by

$$p_f(t_o, t_s) = \Pr(g(\mathbf{X}, t) < 0, \exists t \in [t_o, t_s])$$

$$= \Phi(w) + \phi(w) \left(\frac{1}{w} - \frac{1}{v}\right)$$

$$(40)$$

where

$$w = \operatorname{sgn}(s_s) \{ 2[-K(s_s)] \}^{\frac{1}{2}}$$
 (41)

$$v = s_s [K''(s_s)]^{\frac{1}{2}}$$
 (42)

in which  $sgn(s_s) = +1, -1$ , or 0, depending on whether  $s_s$  is positive, negative, or zero.

The detailed steps of time-dependent component reliability analysis using SOSPA are summarized below.

Step 1: Set k=1. Use the initial time instant as the initial extreme value time  $\tilde{t}^{(0)}=t_0$  and use a unit vector as the initial MPP  $\mathbf{u}_{(1)}^*=\mathbf{u}_0$ .

Step 2: Search for the MPP at time instant  $\tilde{t}^{(k-1)}$  and obtain MPP  $\mathbf{u}_{(k)}^*$  in the k-th cycle by solving

$$\begin{cases} \min \sqrt{\mathbf{U}^{\mathrm{T}}}\mathbf{U} \\ \text{s. t. } g(\mathbf{T}(\mathbf{U}), \tilde{t}^{(k-1)}) = 0 \end{cases}$$

Step 3: Determine the optimal time  $\tilde{t}^{(k)}$  and the corresponding minimum value  $g_{\min}^{(k)}$  by implementing EGO method with  $\mathbf{u}_{(k)}^*$ .

Step 4: Check convergence. The convergence criterion is defined as

$$\varepsilon = \left| g_{\min}^{(k)} \right| \le \varepsilon_{tol}$$

If  $\varepsilon \le \varepsilon_{tol}$ , terminate the iteration. Otherwise, set k=k+1 and return to Step 2.

Step 5: Determine the gradient  $\nabla G$  and Hessian matrix **H** of the envelope function at  $\mathbf{u}_{(k)}^*$  and  $\tilde{t}^{(k)}$ .

Step 6: Calculate  $p_f$  using SOSPA.

Note that the proposed method does not work when the extreme value of the limit-state function occurs at the beginning time instant  $t_o$  or end time instant  $t_s$ , where Eq. (29) is invalid.

### 3.3 System reliability with SOSPA

In this section, we discuss how to extend SOSPA for time dependent component reliability to time dependent system reliability analysis.

System reliability can be estimated by integrating the joint PDF of all responses in the safe region. To use SOSPA, we consider the PDF of component responses directly. The system state is determined by component states predicted from component limit-state functions  $Y_i = g_i(\mathbf{X}, t)$  (i = 1, 2, ... m).

Given all the limit-state functions with time, the series system reliability is then determined by the

$$R_S = \Pr\left(\bigcap_{i=1}^m Y_i = g_i(\mathbf{X}, t) > 0, \forall t \in [t_0, t_s]\right)$$

$$\tag{43}$$

Eq. (43) enable us to consider component reliability and dependencies since it needs the joint PDF  $f_{\mathbf{Y}}(\mathbf{y})$  of  $\mathbf{Y} = (Y_1, Y_2, ..., Y_m)$ . We approximate the joint PDF  $f_{\mathbf{Y}}(\mathbf{y})$  by a multivariate normal distribution. If we only consider the first order terms of the extreme limit-state function Eq. (25), it becomes

$$G_i(\mathbf{U}) = -\nabla G(\mathbf{u}_i^*)^{\mathrm{T}} \mathbf{u}_i^* + \nabla G(\mathbf{u}_i^*)^{\mathrm{T}} \mathbf{U}$$
(44)

If we divide both sides of Eq. (44) by the magnitude of the gradient, we obtain

$$\frac{G_i(\mathbf{U})}{\|\nabla G(\mathbf{u}_i^*)\|} = -\frac{\nabla G_i(\mathbf{u}_i^*)^{\mathrm{T}}}{\|\nabla G(\mathbf{u}_i^*)\|} \mathbf{u}_i^* + \frac{\nabla G_i(\mathbf{u}_i^*)^{\mathrm{T}}}{\|\nabla G(\mathbf{u}_i^*)\|} \mathbf{U}$$
(45)

or

$$\frac{G_i(\mathbf{U})}{\|\nabla G(\mathbf{u}_i^*)\|} = -\alpha_i^{\mathrm{T}} \mathbf{u}_i^* + \alpha_i^{\mathrm{T}} \mathbf{U}$$
(46)

where  $\alpha_i$  is the unit vector of  $\nabla G_i(\mathbf{u}_i^*)$ . At the MPP, the reliability index is given by

$$\mathbf{u}_i^* = -\beta_i \mathbf{\alpha}_i \tag{47}$$

Then event of the safe component  $G_i(\mathbf{U}) > 0$  is equivalent to the event  $\beta_i + \alpha_i^T \mathbf{U} > 0$ . We then define a new variable

$$Z_i = \beta_i + \mathbf{\alpha}_i^{\mathrm{T}} \mathbf{U} \tag{48}$$

 $Z_i$  is an equivalent component response. It is obvious that  $Z_i$  follows a normal distribution. As a result, all the equivalent component responses follow a multivariate normal distribution if the envelope functions of all the components are linearized at their MPPs. The system reliability is then approximated by

$$R_S = \Pr\left(\bigcap_{i=1}^m = -Z_i(\mathbf{U}) < 0\right) \tag{49}$$

 $\mathbf{Z} = (Z_1, Z_2, ..., Z_m)^{\mathrm{T}}$  follows a multivariate normal distribution denoted by  $N(\boldsymbol{\mu}_Z, \boldsymbol{\Sigma}_Z)$ , where  $\boldsymbol{\mu}_Z$  is the mean vector and  $\boldsymbol{\Sigma}_Z$  is the covariance matrix.  $-\mathbf{Z}$  also follows a multivariate normal

distribution  $N(-\mu_Z, \Sigma_Z)$ . System reliability thus becomes the CDF  $\Phi_m(\mathbf{0}; -\mu_Z, \Sigma_Z)$  of  $-\mathbf{Z}$  at  $\mathbf{0}$ ; namely

$$R_S = \Phi_m(\mathbf{0}; -\boldsymbol{\mu}_Z, \boldsymbol{\Sigma}_Z) = \int_{-\infty}^0 \cdots \int_{-\infty}^0 f_z(\mathbf{z}) d\mathbf{z}$$
 (50)

where  $f_z(\mathbf{z})$  is the joint PDF of  $-\mathbf{Z}$ , given by

$$f_Z(\mathbf{z}) = \frac{1}{\sqrt{(2\pi)^m |\mathbf{\Sigma}_Z|}} \exp\left(-\frac{(\mathbf{z} - \mathbf{u}_Z)^T \mathbf{\Sigma}^{-1} (\mathbf{z} - \mathbf{u}_Z)}{2}\right)$$
(51)

The accuracy of the mean vector  $\mu_Z$  and covariance matrix  $\Sigma_Z$  determines the accuracy of the multivariate normal integration in Eq. (51). To maintain high accuracy, we use SOSPA to determine  $\mu_Z$ . The marginal CDF of  $Z_i$  at 0, which is the component reliability is given by

$$R_{\text{SPA}i} = \Pr(Z_i > 0) \tag{52}$$

Then the associated reliability index is determined by

$$\beta_{\text{SPA}i} = \Phi^{-1}(R_{\text{SPA}i}) \tag{53}$$

and  $\beta_{SPAi}$  is an equivalent reliability index.

Since  $\beta_{SPA}$  is estimated with higher accuracy in the estimated reliability, we use it to replace  $\beta$  in Eq. (48). The mean vector of the multivariable distribution of **Z** becomes

$$\mathbf{u}_Z = (\beta_{\text{SPA1}}, \dots, \beta_{\text{SPA}m}) \tag{54}$$

The above treatment ensures that the component reliability or the marginal distributions of component responses are accurately estimated by the second order approximation. For higher efficiency, we use FORM or Eq. (48) to estimate the covariance matrix  $\Sigma_Z$  [33]. Let the components of  $\Sigma_Z$  be  $\rho_{ij}$  ( $i \neq j$ , i,j = 1,2,...,m), which is given by

$$\rho_{ij} = \boldsymbol{\alpha}_i^{\mathrm{T}} \boldsymbol{\alpha}_j \tag{55}$$

Then  $\Sigma_Z$  is given by

$$\mathbf{\Sigma}_{Z} = \begin{bmatrix} 1 & \cdots & \rho_{1m} \\ \vdots & \ddots & \vdots \\ \rho_{m1} & \cdots & 1 \end{bmatrix}_{m \times m}$$
 (56)

With  $\mathbf{u}_Z$  and  $\mathbf{\Sigma}_Z$  available, the system reliability  $R_s$  can be easily calculated by integrating the joint PDF in Eq. (51) from  $(-\infty, ..., -\infty)$  to (0, ..., 0) and the time dependent probability of system failure is

$$p_{fs} = 1 - R_s \tag{57}$$

Many methods such as the first order multi-normal approximation (FOMN) [34] and Alan Genz method [35-37] are developed to integrate  $f_Z(\mathbf{z})$  in Eq. (51). More details about the accuracy of the multivariate normal CDF are given in the Appendix.

The proposed method provides a new way to estimate the time dependent system reliability with nonlinear limit-state functions. The dependencies between component responses are automatically accommodated in the system covariance matrix, and component marginal CDFs can be obtained accurately using SOSPA. The procedure of the system reliability analysis is briefly summarized below. The flowchart of this procedure is given in Fig. 2.

Place Fig. 2 here

Fig. 2 Flowchart of time-dependent system reliability

Step 1: Transform random variables **X** into **U** in the standard normal space.

Execute Step 2 and 4 for all components in the system.

Step 2: Search for MPPs  $\mathbf{u}^*$ , obtain the optimal time  $\tilde{t}$  of the component limit-state function with the efficient global optimization method.

Step 3: Determine the gradient  $\nabla G$  and Hessian matrix **H** of the envelope function.

Step 4: Calculate the probability of component failure and use SOSPA to find the mean vector of equivalent component responses.

Execute Steps 5 and 6 for system reliability analysis.

Step 5: Use the MPPs and reliability indexes of all components to find the covariance matrix of component responses.

Step 6: Form the multivariate normal PDF and integrate it to obtain time dependent system reliability.

### 3.4 Extension to the problems with input random process

When the limit-state function involves random processes, it becomes  $Y = g(\mathbf{X}, \mathbf{L}(t), t)$ , where  $\mathbf{L}(t)$  is a vector of random processes. Series expansion methods, such as the Karhunen-Loeve series expansion, the orthogonal series expansion, and the expansion optimal linear estimation method (EOLE) [38], can be used to convert them into independent random variables, and then the proposed method can still work. Take EOLE as an example for a Gaussian random process L(t). The time interval  $[t_0, t_s]$  is evenly discretized into N points, and the  $N \times N$  autocorrelation coefficient matrix  $\mathbf{\Sigma} = [\rho(t_i, t_j)]$ , i = 1, 2, ..., N, j = 1, 2, ..., N is obtained. Then the EOLE expansion is given by

$$L(\mathbf{U},t) \approx \mu(t) + \sigma(t) \sum_{j=1}^{r} \frac{U_k}{\sqrt{\lambda_j}} \mathbf{\phi}_j^{\mathrm{T}} \mathbf{\Sigma}(:,t), k = 1,2,...,r$$
 (58)

where  $\mu$  (t) and  $\sigma$ (t) are mean and standard deviation of  $\mathbf{L}(t)$ , respectively.  $U_k$ , k=1,2,...r, are independent standard normal variables,  $\lambda = (\lambda_1, \lambda_2, ..., \lambda_r)^T$  is the eigenvalue vector, and  $\boldsymbol{\Phi}_1, \boldsymbol{\Phi}_2, ..., \boldsymbol{\Phi}_r$  are the corresponding eigenvectors obtained from autocorrelation coefficient matrix  $\boldsymbol{\Sigma}$ . Note that r is determined as the smallest integer that meets the following criterion:

$$\frac{\sum_{j=1}^{r} \lambda_j}{\sum_{j=1}^{N} \lambda_j} \ge \eta \tag{59}$$

where  $\eta$  is a hyperparameter determining the accuracy of the expansion. It takes a value close to, but not larger than 1. The smaller is  $\eta$ , the less accurate is the expansion. If  $\eta = 1$ , the expansion is exact. Normally,  $\eta$  is set to 0.9999.

#### 3.5 Parallel Systems

The above results can be extended to parallel systems. For a parallel system, the probability of failure can be computed by

$$p_{fS} = \Pr\left(\bigcup_{i=1}^{m} Y_i = g_i(\mathbf{X}, t) < 0, \exists t \in [t_0, t_s], i = 1, 2, ..., m\right)$$
(60)

Let  $G_i(\mathbf{X}, t) = -g_i(\mathbf{X}, t)$ , then

$$p_{fS} = \Pr\left(\bigcap_{i=1}^{m} Y_i = G_i(\mathbf{X}, t) > 0, \exists t \in [t_0, t_s], i = 1, 2, ..., m\right)$$
(61)

Eq. (61) evaluates the probability of an intersection of m events as Eq. (43) does for a series system. Hence the proposed method can be used to calculate Eq. (61), which leads to the system reliability  $R_S = 1 - p_{fS}$ .

#### 4. EXAMPLES

In this section, three examples are presented to test SOSPA for system reliability analysis. Example 1 is a mathematical problem which is used to demonstrate the details of the proposed method. Examples 2 and 3 are engineering problems. The accuracy is measured by the percentage error with respect to a solution from MCS. The error is calculated by

$$\varepsilon = \frac{\left| p_{fs} - p_{fs}^{\text{MCS}} \right|}{p_{fs}^{\text{MCS}}} \times 100\% \tag{62}$$

where  $p_{fs}$  is the result from SOSPA or FORM, and  $p_{fs}^{MCS}$  is the result from MCS.

### 4.1 Example 1: A math problem

A series system consists of two components with random basic variables  $\mathbf{X} = (X_1, X_2)$ .  $X_i$  (i = 1,2) is normally distributed with parameter  $\mu_i = 3.5$  and  $\sigma_i = 0.3$ . The two limit-state functions are given by

$$g_1(\mathbf{X}, t) = X_1^2 X_2 - 5X_1 t + (X_2 + 1)t^2 - 8.2 \tag{63}$$

$$g_2(\mathbf{X}, t) = (\cos(5^\circ) X_1 + \sin(5^\circ) X_2)^2 (-\sin(5^\circ) X_1 + \cos(5^\circ) X_2)$$

$$-5(\cos(5^\circ) X_1 + \sin(5^\circ) X_2) t + ((-\sin(5^\circ) X_1 + \cos(5^\circ) X_2 + 1) t^2 - 3.9$$
(64)

where t varies within [0,5].

Fig. 3 shows the parabolic curve of the envelope function of  $g_1(\mathbf{X},t)$  formed by the instantaneous limit-state surface at different time instants within the interval [0,5]. The contours of the analytical envelope functions of  $G_1$  and  $G_2$  are plotted in Fig. 4. The shaded area represents the system failure region.

In order to explain clearly how the SOSPA method works, we only show the details for  $g_1(\mathbf{X}, t)$ . First, the MPP of the envelope function at  $\tilde{t}$  is obtained using sequential EGO. The iteration history is shown in Table 1. Once the iteration is convergent, the MPP is found at  $(-1.0714, -3.1172)^{\mathrm{T}}$ .

Fig. 3 Envelope function formed by instantaneous limit-state surfaces



Fig. 4 System extreme limit-state function

The probabilities of failure for  $g_1$  and  $g_2$  from SOSPA are  $p_{f1} = 6.0040 \times 10^{-4}$  and  $p_{f2} = 7.2248 \times 10^{-4}$ . The mean values of the two equivalent component responses  $\mathbf{Z} = (Z_1, Z_2)^{\mathrm{T}}$  are then given by  $\mathbf{u}_{\mathrm{Z}} = \mathbf{\beta}_{\mathrm{SOSPA}} = (-3.2387, -3.1855)^{\mathrm{T}}$ . The unit directional vectors of the two limit-state functions are  $\mathbf{\alpha}_1 = (0.3254, 0.9456)^{\mathrm{T}}$  and  $\mathbf{\alpha}_2 = (0.0098, 1.0)^{\mathrm{T}}$ . Thus, the correlation coefficient between  $g_1$  and  $g_2$  is  $\rho_{12} = \mathbf{\alpha}_1^{\mathrm{T}} \mathbf{\alpha}_2 = 0.9487$ , and the covariance matrix is obtained as follow.

$$\mathbf{\Sigma}_{\mathbf{z}} = \begin{bmatrix} 1 & \rho_{12} \\ \rho_{21} & 1 \end{bmatrix} = \begin{bmatrix} 1 & 0.9487 \\ 0.9487 & 1 \end{bmatrix}$$

Table 1 Iteration history of MPP search for  $g_1$ 

The probability of system failure from SOSPA is  $p_{fs} = 1 - R_s = 9.4747 \times 10^{-4}$ . When FORM is used, the covariance is the same as  $\Sigma_z$ , and the mean values of the two equivalent component responses are below

$$\mathbf{u}_{z} = \mathbf{\beta}_{FORM} = (-3.2963, -3.2079)^{T}$$

The probability of system failure from FORM is  $p_{fs} = 8.3738 \times 10^{-4}$ . The MCS solution with a sample size of  $10^6$  is also obtained. For MCS, the time interval [0,5] is evenly discretized into 100 points. The total number of function calls is therefore  $2 \times 10^8$ . The results are shown in Table 2 where the errors calculated by Eq. (62) are given in brackets. Table 2 shows that SOSPA is much more accurate than FORM which produces a large error due to the nonlinearity of the envelope functions. However, the total function calls of FORM and SOSPA are 365 and 410, respectively, showing FORM is more efficient.

Table 2 Probability of system failure in Example 1

Place Table 2 here

### 4.2 Example 2: A roof truss structure

A roof truss problem is modified as our second example shown in Fig. 5 [39]. The top boom and all the compression bars are made of concrete while the bottom boom and all the tension bars are made of steel. The bars bear a nonstationary Gaussian process whose autocorrelation coefficient function is given by

$$\rho(t_1, t_2) = \exp\left[-\left(\frac{t_1 - t_2}{6}\right)^2\right]$$
 (65)

 $A_C$  and  $E_C$  are the cross-sectional area and elastic modulus of the concrete bars, respectively.  $A_S$  and  $E_S$  are the cross-sectional area and elastic modulus of the steel bars, respectively. All parameters are independent and are listed in Table 3.

Place Fig. 5 here

Fig. 5 A roof truss

Table 3 Distribution of random variables

Place Table 3 here

The perpendicular deflection of the roof peak node is calculated by

$$\Delta C = \frac{ql^2}{2} \left( \frac{3.81}{A_C E_C} + \frac{1.13}{A_S E_S} \right) \tag{66}$$

A failure occurs when the perpendicular deflection  $\Delta C$  exceeds 1.6 cm at any instant of time period [0,10]. The limit-state function is then defined by

$$g_1(\mathbf{X}, t) = 0.016 - \frac{ql^2}{2} \left( \frac{3.81}{A_C E_C} + \frac{1.13}{A_S E_S} \right)$$
 (67)

The second failure mode is that the internal force of one bar exceeds its ultimate stress. The internal force of the bar is 1.185ql, and the ultimate strength of the bar is  $f_CA_C$ , where  $f_C$  is the compressive stress of the bar. The second limit-state function is then given by

$$g_2(\mathbf{X}, t) = f_C A_C - 1.185ql \tag{68}$$

The third failure occurs when the internal force of another bar 0.75ql exceeds its ultimate stress  $f_SA_S$ , where  $f_S$  is the tensile strength of the bar. Therefore, the third limit-state function is formulated by

$$g_3(\mathbf{X}, t) = f_S A_S - 0.75ql \tag{69}$$

The time period [0,10] years is evenly discretized into N=50 points. With Eq. (65), the  $50 \times 50$  autocorrelation coefficient matrix  $\Sigma$  of random process q is obtained. The most significant five eigenvalues of  $\Sigma$  are 35.54, 11.90, 2.24, 0.28, and 0.03. We use EOLE to generate the series expansion of q(t) and only keep the first five orders.

SOSPA produces mean vector of the equivalent component responses:

$$\mu_z = (-2.6681, -3.4056, -2.7416)^{\mathrm{T}}$$

and the covariance matrix is as follows:

$$\mathbf{\Sigma}_{\mathbf{z}} = \begin{bmatrix} 1 & \rho_{12} & \rho_{13} \\ \rho_{21} & 1 & \rho_{23} \\ \rho_{31} & \rho_{32} & 1 \end{bmatrix} = \begin{bmatrix} 1 & 0.1564 & 0.2824 \\ 0.1564 & 1 & 0.0375 \\ 0.2824 & 0.0375 & 1 \end{bmatrix}$$

The probability of system failure from SOSPA is  $p_{fs} = 7.1017 \times 10^{-3}$ .

FORM and MCS are also used, and the sample size of MCS for each component is  $5 \times 10^8$ . The results from three methods are given in Table 4, showing that SOSPA has the higher accuracy than FORM with less efficiency.

Table 4 Probability of system failure in Example 2

### 4.3 Example 3: A Function Generator Mechanism System

Fig. 6 shows a function generator mechanism system, which can achieve a desire motion. This system consists of two function generator mechanisms [40].

Fig. 6 A Function Generator Mechanism System

Mechanism 1 is a four-bar linkage mechanism with links  $B_1$ ,  $B_2$ ,  $B_3$ , and  $B_4$ , and it generates a sine function. Its motion error is the difference between the actual motion output and the required motion output. It is defined as

$$\varepsilon_1(\mathbf{X}_1, \gamma) = \kappa_a(\mathbf{X}_1, \gamma) - \kappa_d(\gamma) \tag{70}$$

where  $\mathbf{X}_1 = (B_1, B_2, B_3, B_4)$  and links  $B_2$  and  $B_5$  are welded together. The two input angles satisfy

$$\gamma = 62^{\circ} + \theta \tag{71}$$

From the mechanism analysis,  $\kappa_a(\mathbf{X}_1, \gamma)$  and  $\kappa_d(\gamma)$  can be obtained by

$$\kappa_a(\mathbf{X}_1, \gamma) = 2 \arctan\left(\frac{-E_1 \pm \sqrt{E_1^2 + D_1^2 - F_1^2}}{F_1 - D_1}\right)$$
(72)

and

$$\kappa_d(\gamma) = 60^\circ + 60^\circ \sin\left(\frac{3}{4}(\gamma - 97^\circ)\right) \tag{73}$$

where  $D_1=2B_4(B_1-B_2cos\gamma)$  ,  $E_1=-2B_2B_4sin\gamma$  , and  $F_1=B_1^2+B_2^2+B_4^2-B_3^2-2B_1B_2cos\gamma$ .

Mechanism 2 is the other four-bar linkage mechanism with links  $B_1$ ,  $B_5$ ,  $B_6$ , and  $B_7$ , and it generates a logarithm function. The motion error is given by

$$\varepsilon_2(\mathbf{X}_2, \theta) = \eta_a(\mathbf{X}_2, \theta) - \eta_d(\theta) \tag{74}$$

where  $\mathbf{X}_2 = (B_1, B_5, B_6, B_7)$ .

$$\eta_a(\mathbf{X}_2, \theta) = 2 \arctan\left(\frac{-E_2 \pm \sqrt{E_2^2 + D_2^2 - F_2^2}}{F_2 - D_2}\right)$$
(75)

$$\eta_d(\theta) = 60^{\circ} \log_{10} \frac{[(\theta + 15^{\circ})/60^{\circ}]}{\log_{10} 2}$$
 (76)

where  $D_2=2B_7(B_1-B_5cos\theta)$  ,  $E_2=-2B_5B_7sin\theta$  , and  $F_2=B_1^2+B_5^2+B_7^2-B_6^2-2B_1B_5cos\theta$ .

Mechanism 1 is considered reliable if  $\{e_2 < \varepsilon_1(\mathbf{X}_1, \gamma) < e_1\}$ , where  $e_1$  and  $e_2$  are allowable motion errors with  $e_1 = 1.4$  and  $e_2 = -0.8$ . When the motion error is positive, the limit-state function is defined by

$$g_1(\mathbf{X}_1, \gamma) = e_1 - \varepsilon_1(\mathbf{X}_1, \gamma) \tag{77}$$

As for the negative motion error, the limit-state function is given by

$$g_2(\mathbf{X}_1, \gamma) = \varepsilon_1(\mathbf{X}_1, \gamma) - e_2 \tag{78}$$

Similarly, the limit-state functions of mechanism 2 are as follows:

$$g_3(\mathbf{X}_2, \theta) = e_3 - \varepsilon_2(\mathbf{X}_2, \theta) \tag{79}$$

$$g_4((\mathbf{X}_2, \theta)) = \varepsilon_2(\mathbf{X}_2, \theta) - e_4$$
 (80)

in which  $e_3=1.0$  and  $e_4=-2.4$ . The random variables are given in Table 5. The mechanism

system performs its intended functions over an interval of  $[\theta_0, \theta_s] = [45^{\circ}, 95^{\circ}]$ . The system is a

series system with four components (limit-state functions).

Table 5 Parameters in Example 3

Place Table 5 here

\_\_\_\_\_

Table 6 shows the results. It indicates that the accuracy of SOSPA is in general better than

FORM. However, both methods produce almost identical results for  $p_{f2}$  and  $p_{f4}$ . The reason is

that the extreme values of two corresponding limit-state functions occur at the beginning of the

time period (at 45°). Thus, the Hessian matrices of the two envelope functions are not accurate,

and SOSPA is not accurate for  $p_{f2}$  and  $p_{f4}$ . Since the two probabilities of component failure are

much smaller than the other two probabilities, their effect on the probability of system failure is

insignificant.

Table 6 Probability of system failure in Example 3

Place Table 6 here \_\_\_\_\_

28

#### 5. CONCLUSION

The proposed time dependent system reliability method predicts system reliability with a second order approximation. It is therefore in general more accurate than the first order approximation method. But it is less efficient than the latter method due to the need of second derivatives.

The new method converts a time dependent problem into a time independent problem by using the envelope function or the extreme value of a limit-state function over the time span under consideration. The most probable point (MPP) of the envelope function is found with the help of efficient global optimization. Then the envelope function is approximated at the MPP with its gradient and Hessian matrix. The reliability of each component is calculated by the second order saddlepoint approximation, and the dependencies between component responses are considered with the first approximation for the sake of efficiency. Once the estimated marginal component distributions and component correlations are available, the joint distribution of all the component responses is formed by a multivariate normal distribution, which leads to a fast evaluation of the system reliability.

The proposed envelope method works well if the envelope function is convex. The global MPP of the envelope function may not be found if the envelope function has multiple MPPs. For this case, the MPP search may start from different instants of time, and then the worst-case MPP is used. The proposed method does not work for a special case where the extreme value of a limit-state function occurs at the beginning or end of the period of time under consideration, and the reason is that the derivations of the Hessian matrix of the envelope function are for the case where the extreme value occurs inside the period of time.

Out future work will address the above two issues. The proposed method can also be further extended to time and space dependent problems where random processes and random fields are also involved.

#### **ACKNOWLEDGEMENTS**

We would like to acknowledge the support from the National Science Foundation under Grants No. 1923799 (formerly 1727329).

### **APPENDIX: Accuracy of Multivariate Normal Integration**

The numerical integration of the multivariate normal probability in Eq. (50) is often a difficult problem if the dimension is high [35]. Here we provide two examples to show the performance of the numerical integration of multivariate normal probability.

The first example is Example 1 in Sec. 4. The mean values of the two equivalent component responses are  $\mu = (-3.2963, -3.2079)^{\rm T}$ , and the covariance matrix is  $\Sigma = \begin{bmatrix} 1 & 0.9487 \\ 0.9487 & 1 \end{bmatrix}$ . This is a low-dimensional problem. We have provided the result from the numerical integration method  $p_{fs} = 8.3737 \times 10^{-4}$ . The results from MCS with a sample size of  $10^8$  is  $p_{fs} = 8.3702 \times 10^{-4}$ . The difference between the two probabilities is 0.04%, indicating the good accuracy of the numerical integration method.

Example 2 involves a time-dependent problem with the limit-state function

$$g(t) = -4 + U_1 \cos(t) + U_2 \sin(t)$$
(81)

where  $t \in [0,2\pi]$ .  $U_1$  and  $U_2$  are standard normal variables. g(t) is a stationary Gaussian process with a mean of -4 and a autocorrelation coefficient function  $\rho(t_1,t_2)$  given by

$$\rho(t_1, t_2) = \cos(t_1 - t_2) \tag{83}$$

If  $t \in [0,2\pi]$  is evenly discretized into 500 points, then g(t) is discretized into 500 random variables  $g_i$ , i = 1,2,...500. With the discretization, Eq. (2) can rewrite as

$$R = \Pr\left(\bigcap_{i=1}^{500} g_i(X, t_i) \ge 0, \forall t_i \in [t_0, t_s]\right)$$
(84)

The normal integration is 500 dimensional. The mean vector  $\mathbf{\mu} = \left(\mu_{g_i}\right)_{i=1,2,\dots,500}^{\mathrm{T}}$  where  $\mu_{g_i} = -4$ . The covariance matrix is  $\mathbf{\Sigma}_g = \left(\rho_{ij}\right)_{i,j=1,2,\dots,500}$  where

$$\rho_{ij} = \begin{cases} \cos(t_i - t_j) & \text{if } i \neq j \\ 1 & \text{if } i = j \end{cases}$$
 (85)

The time-dependent probability of failure  $p_f = 1 - R$ .

For this high-dimensional normal integration, the commonly used method is the Quasi MCS method [37]. The analytical solution exists for this problem and is given in Table A.1. If a special treatment is implemented for this problem, for example, the dimension reduction by eliminating the time instants where the  $\Pr(g_i(X, t_i) \ge 0)$  is low, the error could be reduced as shown in Table A.1.

Table A.1 Results of high dimensional normal integration

Method	Exact	Quasi MCS method	Dimension reduction method
$p_{fs}$	$3.3546 \times 10^{-4}$	$4.3109 \times 10^{-4}$ (28.5%)	$3.3370 \times 10^{-4}$ (0.5%)

The two examples indicate that a low dimensional ( $\leq 3$ ) normal integration can be computed by numerical integration with good accuracy. A higher dimensional normal integration may not be accurate. Obtaining high accuracy of higher dimensional normal integrations deserves further investigations.

#### REFERENCES

- [1] Rausand, M., and Høyland, A., 2003, System reliability theory: models, statistical methods, and applications, John Wiley & Sons.
- [2] Hu, Z., and Du, X., 2014, "Lifetime cost optimization with time-dependent reliability," Engineering Optimization, 46(10), pp. 1389-1410.
- [3] Singh, A., Mourelatos, Z. P., and Li, J., 2010, "Design for lifecycle cost using time-dependent reliability," Journal of Mechanical Design, 132(9), p. 091008.
- [4] Wu, H., Zhu, Z., and Du, X., 2020, "System Reliability Analysis with Autocorrelated Kriging Predictions," Journal of Mechanical Design, 142(10), p. 101702.
- [5] Zhang, J., and Du, X., 2011, "Time-dependent reliability analysis for function generator mechanisms," Journal of Mechanical Design, 133(3), p. 031005.
- [6] Caprani, C. C., and OBrien, E. J., 2010, "The use of predictive likelihood to estimate the distribution of extreme bridge traffic load effect," Structural safety, 32(2), pp. 138-144.
- [7] Hu, Z., and Du, X., 2012, "Reliability analysis for hydrokinetic turbine blades," Renewable Energy, 48, pp. 251-262.
- [8] Andrieu-Renaud, C., Sudret, B., and Lemaire, M., 2004, "The PHI2 method: a way to compute time-variant reliability," Reliability Engineering & System Safety, 84(1), pp. 75-86.
- [9] Hu, Z., and Du, X., 2013, "Time-dependent reliability analysis with joint upcrossing rates," Structural and Multidisciplinary Optimization, 48(5), pp. 893-907.
- [10] Jiang, C., Wei, X. P., Huang, Z. L., and Liu, J., 2017, "An Outcrossing Rate Model and Its Efficient Calculation for Time-Dependent System Reliability Analysis," Journal of Mechanical Design, 139(4), pp. 041402-041402-041410.
- [11] Hu, Z., Li, H., Du, X., and Chandrashekhara, K., 2013, "Simulation-based time-dependent reliability analysis for composite hydrokinetic turbine blades," Structural and Multidisciplinary Optimization, 47(5), pp. 765-781.
- [12] Hu, Z., and Mahadevan, S., 2016, "A single-loop kriging surrogate modeling for time-dependent reliability analysis," Journal of Mechanical Design, 138(6), p. 061406.
- [13] Hu, Z., and Du, X., 2015, "Mixed efficient global optimization for time-dependent reliability analysis," Journal of Mechanical Design, 137(5), p. 051401.
- [14] Wang, Z., and Wang, P., 2013, "A new approach for reliability analysis with time-variant performance characteristics," Reliability Engineering & System Safety, 115, pp. 70-81.
- [15] Rice, S. O., 1944, "Mathematical analysis of random noise," Bell System Technical Journal, 23(3), pp. 282-332.
- [16] Du, X., 2014, "Time-dependent mechanism reliability analysis with envelope functions and first-order approximation," Journal of Mechanical Design, 136(8), p. 081080.

- [17] Li, J., Chen, J.-b., and Fan, W.-l., 2007, "The equivalent extreme-value event and evaluation of the structural system reliability," Structural safety, 29(2), pp. 112-131.
- [18] Singh, A., and Mourelatos, Z. P., 2010, "On the time-dependent reliability of non-monotonic, non-repairable systems," SAE International Journal of Materials and Manufacturing, 3(1), pp. 425-444.
- [19] Hu, Z., and Du, X., "Second Order Reliability Method for Time-Dependent Reliability Analysis Using Sequential Efficient Global Optimization," Proc. ASME 2019 International Design Engineering Technical Conferences and Computers and Information in Engineering Conference, American Society of Mechanical Engineers Digital Collection.
- [20] Song, J., and Der Kiureghian, A., 2006, "Joint first-passage probability and reliability of systems under stochastic excitation," Journal of Engineering Mechanics, 132(1), pp. 65-77.
- [21] Radhika, B., Panda, S., and Manohar, C., 2008, "Time variant reliability analysis of nonlinear structural dynamical systems using combined Monte Carlo simulations and asymptotic extreme value theory," Computer Modeling in Engineering and Sciences, 27(1/2), p. 79.
- [22] Yu, S., Wang, Z., and Meng, D., 2018, "Time-variant reliability assessment for multiple failure modes and temporal parameters," Structural and Multidisciplinary Optimization, 58(4), pp. 1705-1717.
- [23] Gong, C., and Frangopol, D. M., 2019, "An efficient time-dependent reliability method," Structural Safety, 81, p. 101864.
- [24] Hu, Z., and Mahadevan, S., 2015, "Time-dependent system reliability analysis using random field discretization," Journal of Mechanical Design, 137(10), p. 101404.
- [25] Jiang, C., Wei, X., Wu, B., and Huang, Z., 2018, "An improved TRPD method for time-variant reliability analysis," Structural and Multidisciplinary Optimization, 58(5), pp. 1935-1946.
- [26] Hohenbichler, M., and Rackwitz, R., 1982, "First-order concepts in system reliability," Structural safety, 1(3), pp. 177-188.
- [27] Wu, H., and Du, X., 2020, "System Reliability Analysis With Second-Order Saddlepoint Approximation," ASCE-ASME J Risk and Uncert in Engrg Sys Part B Mech Engrg, 6(4).
- [28] Hu, Z., and Du, X., 2015, "Mixed efficient global optimization for time-dependent reliability analysis," Journal of Mechanical Design, 137(5), p. 051401.
- [29] Jones, D. R., Schonlau, M., and Welch, W. J., 1998, "Efficient global optimization of expensive black-box functions," Journal of Global optimization, 13(4), pp. 455-492.
- [30] Wang, Z., and Wang, P., 2012, "A nested extreme response surface approach for time-dependent reliability-based design optimization," Journal of Mechanical Design, 134(12). p. 121007.
- [31] Goutis, C., and Casella, G. J. A. S., 1999, "Explaining the Saddlepoint Approximation," American Statistician, 53(3), pp. 216-224.
- [32] Hu, Z., and Du, X., 2018, "Saddlepoint approximation reliability method for quadratic functions in normal variables," Structural Safety, 71, pp. 24-32.
- [33] Zeng, P., Jimenez, R., Li, T., Chen, Y., and Feng, X., 2017, "Application of Quasi-Newton Approximation-Based SORM for System Reliability Analysis of a Layered Soil Slope," Geo-Risk 2017, pp. 111-119.
- [34] Gollwitzer, S., and Rackwitz, R., 1988, "An efficient numerical solution to the multinormal integral," Probabilistic Engineering Mechanics, 3(2), pp. 98-101.
- [35] Genz, A., 1992, "Numerical computation of multivariate normal probabilities," Journal of computational and graphical statistics, 1(2), pp. 141-149.

- [36] Genz, A., 2004, "Numerical computation of rectangular bivariate and trivariate normal and t probabilities," Statistics and Computing, 14(3), pp. 251-260.
- [37] Genz, A., and Bretz, F., 2009, Computation of multivariate normal and t probabilities, Springer Science & Business Media.
- [38] Li, C.-C., and Der Kiureghian, A., 1993, "Optimal discretization of random fields," Journal of engineering mechanics, 119(6), pp. 1136-1154.
- [39] Wei, P., Liu, F. and Tang, C., 2018, "Reliability and reliability-based importance analysis of structural systems using multiple response Gaussian process model," Reliability Engineering & System Safety, 175, pp.183-195.
- [40] Hu, Z., Zhu, Z., and Du, X., 2017, "Time-Dependent System Reliability Analysis for Bivariate Responses," ASCE-ASME J Risk and Uncert in Engrg Sys Part B Mech Engrg, 4(3).

## **List of Table Captions**

**Table 1** Iteration history of MPP search for  $g_1$ 

**Table 2** Probability of system failure in Example 1

**Table 3** Distribution of random variables

**Table 4** Probability of system failure in Example 2

**Table 5** Parameters in Example 3

**Table 6** Probability of system failure in Example 3

## **List of Figure Captions**

- Fig. 1 Relationship between the worst-case limit-state function and envelope function
- Fig. 2 Flowchart of time-dependent system reliability
- Fig. 3 Envelope function formed by instantaneous limit-state surfaces
- Fig. 4 System extreme limit-state function
- Fig. 5 A roof truss
- Fig. 6 A Function Generator Mechanism System

Table 1 Iteration history of MPP search for  $g_1$ 

Iterations	u*	ĩ
1	$(-6.1450, -1.7052)^{\mathrm{T}}$	1.4735
2	$(-2.1526, -2.9252)^{\mathrm{T}}$	1.9689
3	$(-1.3877, -3.0305)^{\mathrm{T}}$	2.1483
4	$(-1.1631, -3.0878)^{\mathrm{T}}$	2.2063
5	$(-1.0941, -3.1096)^{\mathrm{T}}$	2.2251
6	$(-1.0714, -3.1172)^{\mathrm{T}}$	2.2314

Table 2 Probability of system failure in Example 1

Methods	SOSPA	FORM	MCS
$p_{f1}$	$6.0040 \times 10^{-4}$ (2.81%)	$4.8989 \times 10^{-4}$ (16.10%)	$5.840 \times 10^{-4}$
$p_{f2}$	$7.2248 \times 10^{-4}$ (3.28%)	$6.6864 \times 10^{-4}$ (10.50%)	$7.470 \times 10^{-4}$
$p_{fs}$	$9.4747 \times 10^{-4} $ (0.89%)	$8.3738 \times 10^{-4}$ (12.40%)	$9.560 \times 10^{-4}$
$N_{calls}$ of $g_1$	127	112	108
$N_{calls}$ of $g_2$	283	253	108
Total	410	365	$2 \times 10^{8}$

Table 3 Distribution of random variables

Variable (Unit)	Mean	Standard deviation	Distribution
q(N/m)	$14000(0.2\sin(0.25t) + 0.8)$	500	Nonstationary Gaussian process
L(m)	12	0.12	Normal
$A_S(\mathrm{m}^2)$	$9.0 \times 10^{-4}$	$9.0 \times 10^{-5}$	Normal
$A_C(\mathrm{m}^2)$	5×10 <sup>-2</sup>	5×10 <sup>-3</sup>	Normal
$E_S(N/m^2)$	2×10 <sup>11</sup>	2×10 <sup>10</sup>	Lognormal
$E_C(N/m^2)$	3×10 <sup>10</sup>	3×10 <sup>9</sup>	Lognormal
$f_S(N/m^2)$	3.35×10 <sup>8</sup>	6.7×10 <sup>7</sup>	Normal
$f_C(N/m^2)$	1.34×10 <sup>7</sup>	2.68×10 <sup>6</sup>	Normal

**Table 4** Probability of system failure in Example 2

Methods	SOSPA	FORM	MCS
$p_{f1}$	$3.8140 \times 10^{-3}$ (3.74%)	$3.4370 \times 10^{-3}$ (13.35%)	$3.9623 \times 10^{-3}$
$p_{f2}$	$3.3010 \times 10^{-4}$ (2.16%)	$3.0768 \times 10^{-4}$ (8.81%)	$3.3740 \times 10^{-4}$
$p_{f3}$	$3.0569 \times 10^{-3}$ (2.41%)	$2.8297 \times 10^{-3}$ (9.66%)	$3.1324 \times 10^{-3}$
$p_{fs}$	$7.1017 \times 10^{-3}$ (2.78%)	$6.4885 \times 10^{-3}$ (11.20%)	$7.3049 \times 10^{-3}$
$N_{calls}$ of $g_1$	306	188	$5 \times 10^{8}$
$N_{calls}$ of $g_1$	599	363	$5 \times 10^{8}$
$N_{calls}$ of $g_1$	592	538	5 × 10 <sup>8</sup>
Total	1797	1089	$1.5 \times 10^{9}$

 Table 5 Parameters in Example 3

Variable (Unit)	Mean	Standard deviation	Distribution
$B_1(mm)$	100	0.3	Normal
$B_2(mm)$	55.5	0.05	Normal
<i>B</i> <sub>3</sub> (mm)	144.1	0.05	Normal
$B_4(\text{mm})$	72.5	0.05	Normal
<i>B</i> <sub>5</sub> (mm)	79.5	0.05	Normal
B <sub>6</sub> (mm)	203	0.05	Normal
<i>B</i> <sub>7</sub> (mm)	150.8	0.05	Normal

Table 6 Probability of system failure in Example 3

Methods	SOSPA	FORM	MCS
$p_{f1}$	$6.8663 \times 10^{-3}$ (1.12%)	$5.6273 \times 10^{-3}$ (18.94%)	$6.9440 \times 10^{-3}$
$p_{f2}$	$6.1088 \times 10^{-5}$ (4.55%)	$6.1088 \times 10^{-5}$ (4.55%)	$6.430 \times 10^{-5}$
$p_{f3}$	$2.5156 \times 10^{-3}$ (0.17%)	$\begin{array}{c} 2.0006 \times 10^{-3} \\ (19.20\%) \end{array}$	$2.520 \times 10^{-3}$
$p_{f4}$	$4.3845 \times 10^{-4}$ (11.80%)	$4.3845 \times 10^{-4} $ (11.80%)	$4.970 \times 10^{-4}$
$p_{fs}$	$7.5580 \times 10^{-3}$ (1.11%)	$6.2230 \times 10^{-3}$ (18.60%)	$7.6430 \times 10^{-3}$
$N_{calls}$ of $g_1$	179	124	108
$N_{calls}$ of $g_2$	398	288	108
$N_{calls}$ of $g_3$	320	210	108
$N_{calls}$ of $g_4$	479	369	108

Total 1376	991	$4 \times 10^{8}$
------------	-----	-------------------

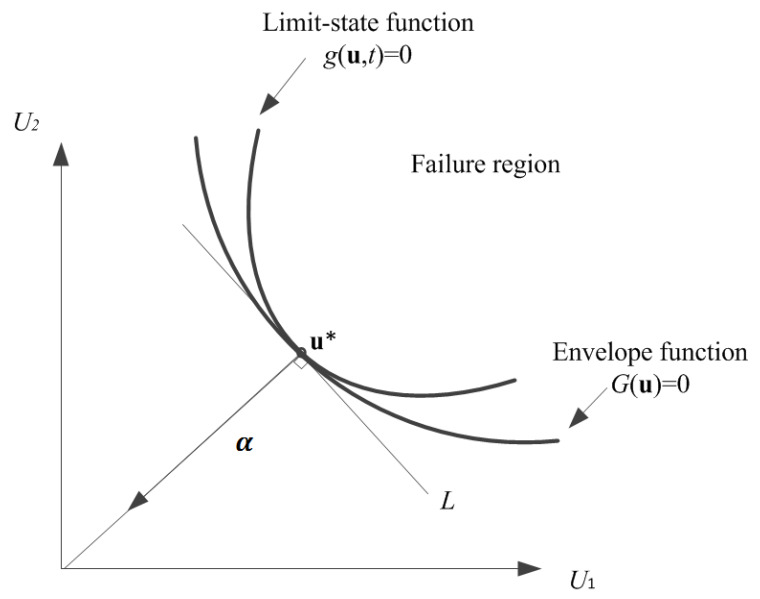


Fig. 1 Relationship between the worst-case limit-state function and envelope function

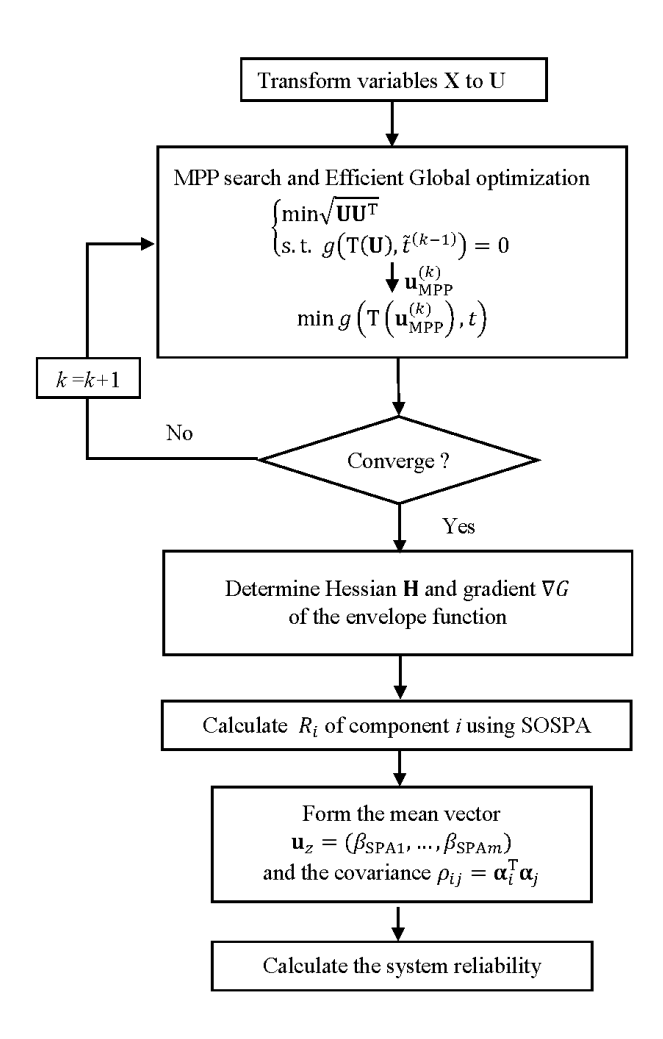


Fig. 2 Flowchart of time-dependent system reliability

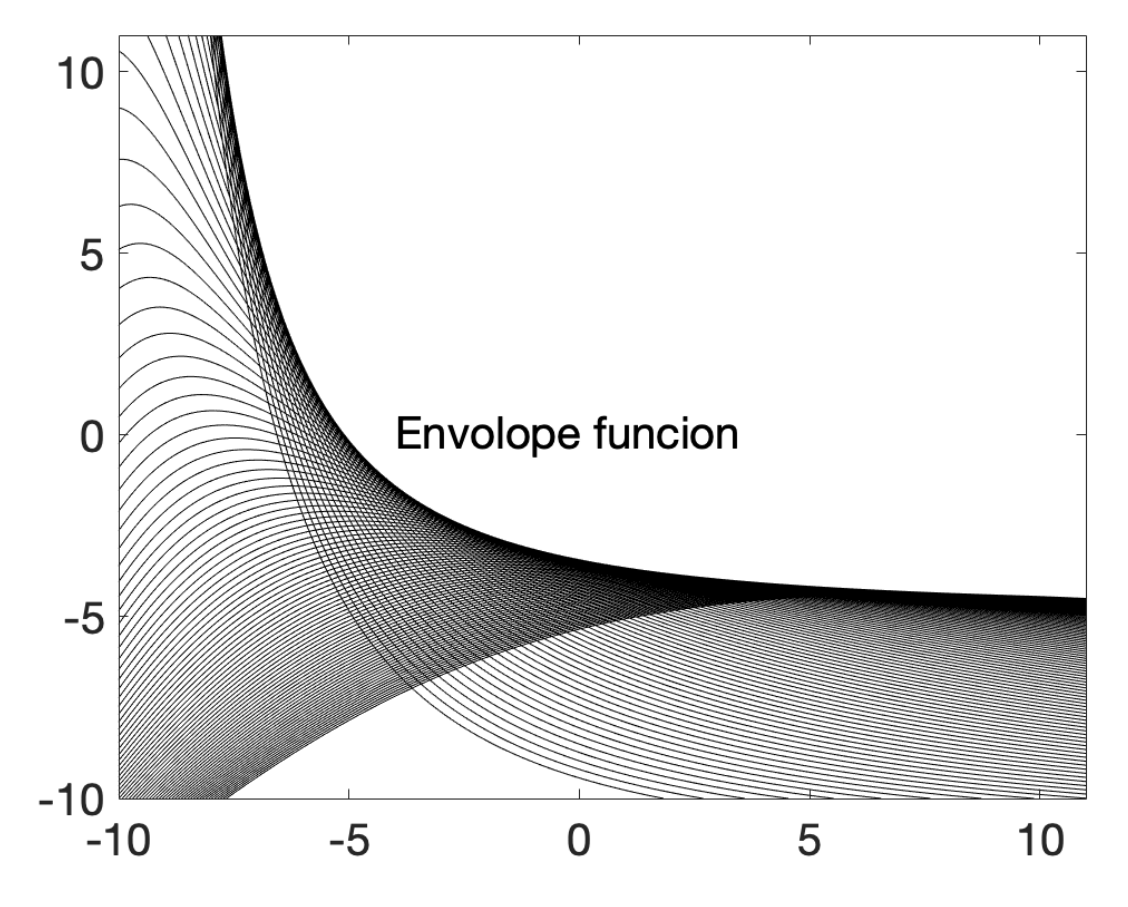


Fig. 3 Envelope function formed by instantaneous limit-state surfaces

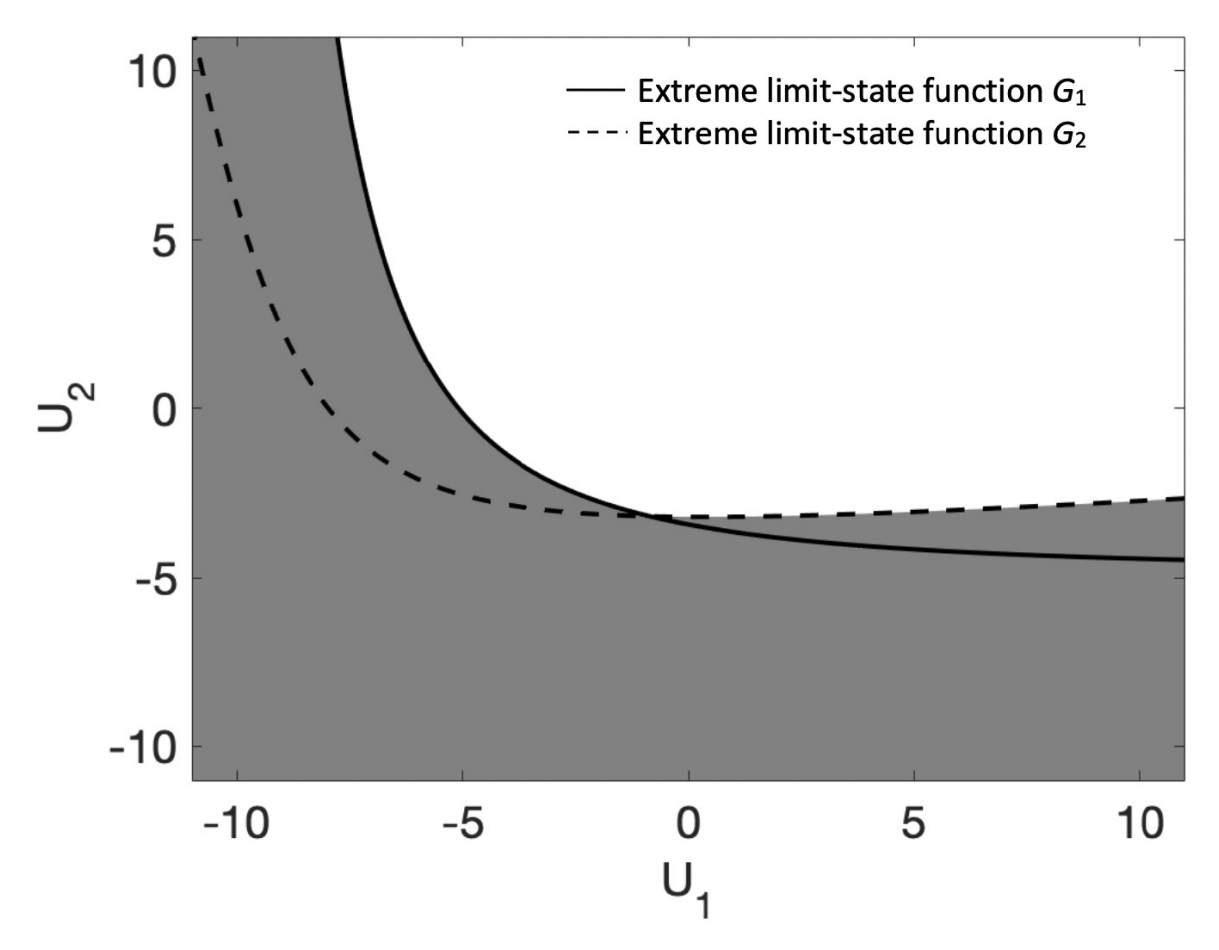
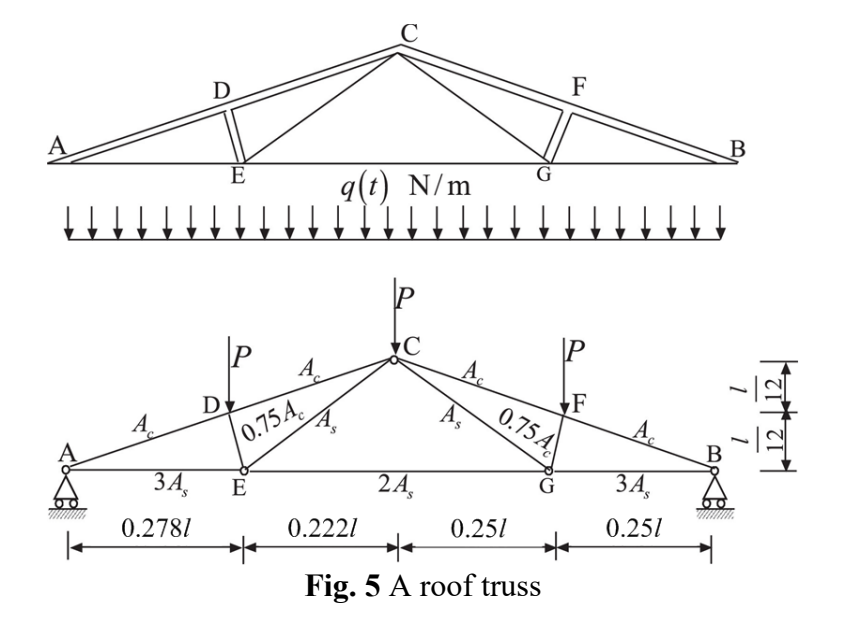


Fig. 4 System extreme limit-state function



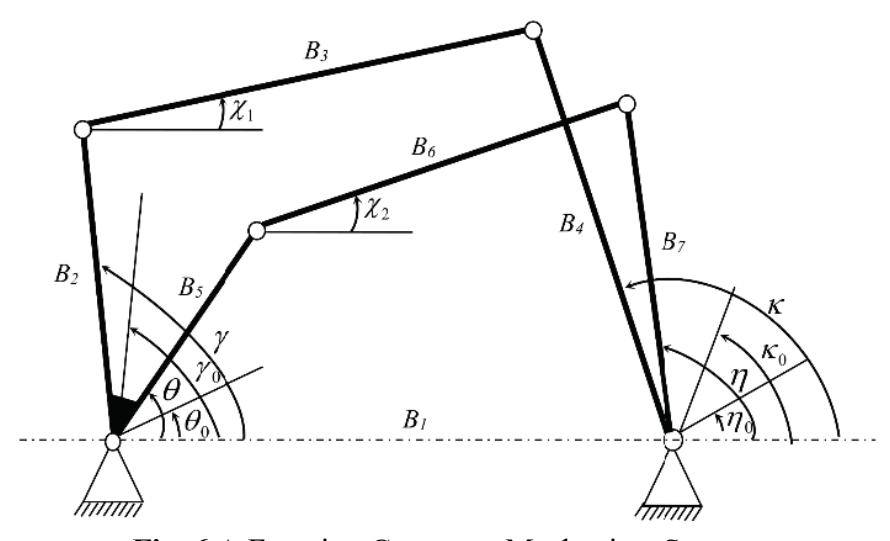


Fig. 6 A Function Generator Mechanism System